

# On the two-dimensional metallic state in silicon-on-insulator structures

G. Brunthaler<sup>a\*</sup>, A. Prinz<sup>a</sup>, G. Pillwein<sup>a</sup>, P.E. Lindelof<sup>b</sup>, J. Ahopelto<sup>c</sup>  
<sup>a</sup> *Institut für Halbleiterphysik, Johannes Kepler Universität, A-4040 Linz, Austria*  
<sup>b</sup> *Niels Bohr Institute, University of Copenhagen, DK-2100 Copenhagen, Denmark*  
<sup>c</sup> *VTT Centre for Microelectronics, Tekniikantie 17, FIN-02150 Espoo, Finland*

(November 15, 2018)

It is shown that the electronic conduction in silicon-on-insulator (SOI) layers exhibits a metallic regime which is very similar to that in high-mobility Si-metal oxide semiconductor structures (MOS). The peak in the electron mobility versus density, the strong drop in resistivity and the critical concentration for the metal-insulator transition are all consistent. On the basis of our SOI data for the temperature and in-plane magnetic field dependence of the resistivity, we discuss several models for the metallic state in two dimensions. We find that the observed behavior can be well described by the theory on the interaction corrections in the ballistic regime. For the investigated regime, the temperature dependent screening of scattering potentials gives also a good description of the data.

## I. INTRODUCTION

The discovery of an apparent metallic state in Si-metal oxide semiconductor (MOS) structures<sup>1</sup> has attracted much attention as it seemed to contradict the two-dimensional (2D) localization behavior<sup>2</sup>. It was found that above a critical carrier concentration  $n_c$ , the resistivity strongly decreases with decreasing temperature  $T$  (metallic regime), whereas it increases for lower densities  $n < n_c$  (insulating regime). The scaling parameter  $T_0$  shows a critical behavior around  $n_c$ <sup>1</sup>.

At first the discovery of the metallic state in two dimensions was met with great scepticism. But the metal-to-insulator transition (MIT) was confirmed first in Si-MOS structures from a different source<sup>3</sup> and further in several other 2D material systems, which are n- and p-SiGe and AlGaAs and n-AlAs structures (for references see<sup>4</sup>).

After these experimental findings, the question was raised whether the metallic behavior manifests a new electronic ground state with dominating quantum behavior or if the strong resistivity drop towards low  $T$  is based on familiar (i.e. non coherent) effects (for a detailed discussion see<sup>4</sup> and references therein).

In this work, we report on the finding of a metallic state in silicon-on-insulator (SOI) structures. In section II, on the experiment, we describe the investigated samples and the setup. We further present the data on the temperature and the magnetic field dependence of the resistivity and we show the mobility versus density behavior. The experimental results of the SOI system are compared in detail with the properties of Si-MOS structures and the differences are discussed. The discussion of the results follows in section III. Here we discuss and compare five

important suggestions on the physical origin of the metallic state in two dimensions. It turns out that the coherent interaction corrections to the conductivity in the ballistic regime<sup>5,6</sup> are able to describe the observed resistivity behavior quite well. For the investigated regime also the temperature dependent screening of scattering potentials<sup>7</sup> gives a fairly good description of the data. After a short summary, we describe in appendix A our numerical calculations on the charged trap state model in detail.

## II. EXPERIMENT

### A. Samples and setup

Our investigations were performed on two high-mobility SOI structures which were prepared recently in Finland. The SOI Hall bars have identical peak mobilities of  $\mu_p = 11,600 \text{ cm}^2/\text{Vs}$ . They were fabricated on commercial 'Unibond' wafers produced by the Smart-Cut process<sup>8</sup>. The thickness of the Si-layer amounts 200 nm and that of the buried oxide layer 400 nm in these wafers. The background doping is n-type of about  $10^{15} \text{ cm}^{-3}$  which freezes out at low temperature. After a two-step thermal oxidation, the final thickness of the Si-layer is 60 nm. The gate oxide thickness is about 90 nm with a dielectric strength of approximately 1 V/nm. The electric contacts were phosphorus-implanted to an activated carrier concentration of  $4 \times 10^{19} \text{ cm}^{-3}$ . The Al-metallization is 300 nm thick and sintered at 400°C. A scheme of the final layer sequence is shown in Figure 1. The etched Hall bars have a size of  $800 \mu\text{m}$  times  $100 \mu\text{m}$  giving a length to width ratio of 8. All resistivity and Hall measure-

---

\*Corresponding author: Tel.: +43-732-24689603; Fax.: +43-732-2468-8650; e-mail: G.Brunthaler@hphys.uni-linz.ac.at

ments were performed in a four terminal AC-technique at low frequencies of typically 13 or 17 Hz. The SOI structures were investigated in a  $^4\text{He}$  cryostat down to 1.4 K. Most investigations were performed on sample number L2, sample L1 showed in several measurements practically the same behavior.

The SOI sample number L2 was intensively investigated in a density range from  $1.3 \times 10^{11}$  to  $1.04 \times 10^{12} \text{ cm}^{-2}$ . At the low density side of this range, the contacts became high ohmic. Due to capacitive effects, the measured voltages showed a delay time of more than 100 ms before they came into a steady state. Thus voltage measurements in DC-technique lead to other values than those with the 13 Hz AC-technique. We limited our measurements to the range where the AC- and DC-technique gave the same results and performed all investigations in the AC-technique as this gives a better signal-to-noise ratio. At the higher limit of the investigated density range, the gate started to leak and the current between gate and sample would have lead to errors in the resistivity calculations. The investigations were thus kept in the above given density range.

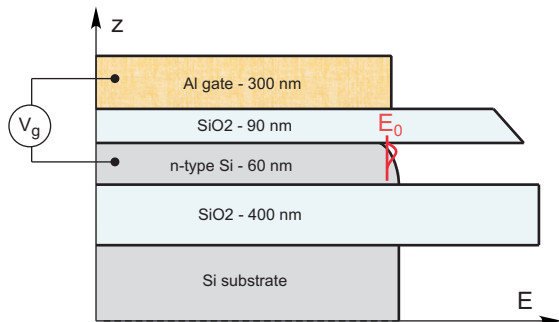


FIG. 1. Scheme of the sample structure for silicon-on-insulator structures. The vertical axis shows the layer sequence (not to scale), the horizontal axis the band offsets.

## B. Resistivity behavior

From the resistivity and Hall measurements, the carrier density  $n$  and the mobility  $\mu$  were calculated assuming the linear Drude behavior to be valid. This is not clear a priori as quantum interference effects might give relevant contributions to the conductivity and would alter the necessary evaluation. The possible importance of quantum effects will be discussed later in this work. For now,  $n$  and  $\mu$  should be used as apparent Drude parameters for the 2D electron gas.

We have evaluated the dependence of mobility  $\mu$  on the electron density  $n$  by varying the gate voltage  $V_g$  at a constant temperature of  $T = 1.5 \text{ K}$ . In Fig. 2, the  $\mu(n)$ -dependence for SOI is compared with that for several Si-MOS samples<sup>9</sup> with different mobilities. The SOI

structure has a peak mobility  $\mu_p$  of  $11,600 \text{ cm}^2/\text{Vs}$  at a density of  $6.5 \times 10^{11} \text{ cm}^{-2}$ . As can be seen from Fig. 2, the Si-MOS samples have lower or higher peak mobilities, depending on the sample quality, but the overall behavior of  $\mu(n)$  is very similar for the two sample types.

At high densities, the electron wave function is squeezed by the strong electric field of the triangular potential towards the gate-sided Si/SiO<sub>2</sub> interface and thus interface roughness scattering dominates. At low  $n$ , the dominating scattering process is caused by impurities. At the transition region between the two scattering mechanisms, the mobility reaches its peak value  $\mu_p$ <sup>10</sup>.

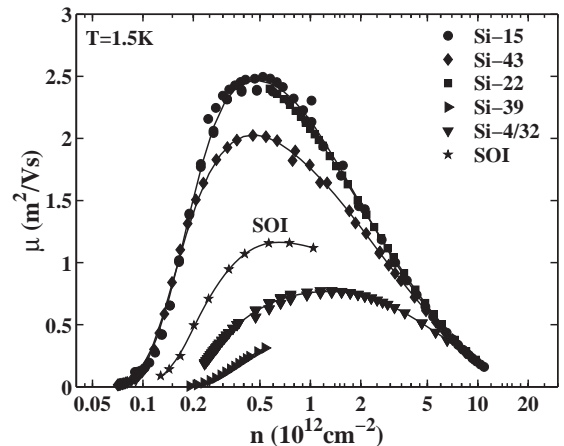


FIG. 2. Mobility  $\mu$  versus density  $n$  for a SOI structure in comparison with several Si-MOS samples at a temperature of 1.5 K.

The most typical feature of the metallic state in 2D systems is expressed by the strong resistivity drop towards lower temperatures. This strong drop in  $\rho(T)$  is clearly visible in Fig. 3b for the SOI sample in the range of  $1.67 \times 10^{11} \leq n \leq 1.04 \times 10^{12} \text{ cm}^{-2}$ . The maximum decrease in  $\rho(T)$  amounts up to about a factor 3.5 for  $n = 2.47 \times 10^{11} \text{ cm}^{-2}$ . For the two lower density curves with  $n = 1.28$  and  $1.44 \times 10^{11} \text{ cm}^{-2}$ , an insulating behavior is observed. The critical concentration  $n_c$ , at which the behavior changes from insulating to metallic, lies at about  $1.55 \times 10^{11} \text{ cm}^{-2}$ .

For comparison, in Fig. 3a and 3c the very high and medium mobility Si-MOS samples<sup>11</sup> Si-15 and Si-4/32 with  $\mu_p = 27,000$  and  $8,000 \text{ cm}^2/\text{Vs}$ , respectively, are shown. In sample Si-15, the strong decrease in  $\rho(T)$  is shifted to lower  $T$  and the maximum decrease amounts up to a factor 7, in Si-4/32 the decrease is at somewhat higher  $T$  in comparison to the SOI structure and the maximum decrease is about a factor 3. This shows a clear trend of the properties of the metallic regime with the sample quality, i.e. the peak mobility  $\mu_p$  and manifests the similarities between SOI and Si-MOS structures. Additionally, in Fig. 3, dashed-dotted lines at  $E_f = k_B T$ ,  $4k_B T$  and  $16k_B T$  are shown.

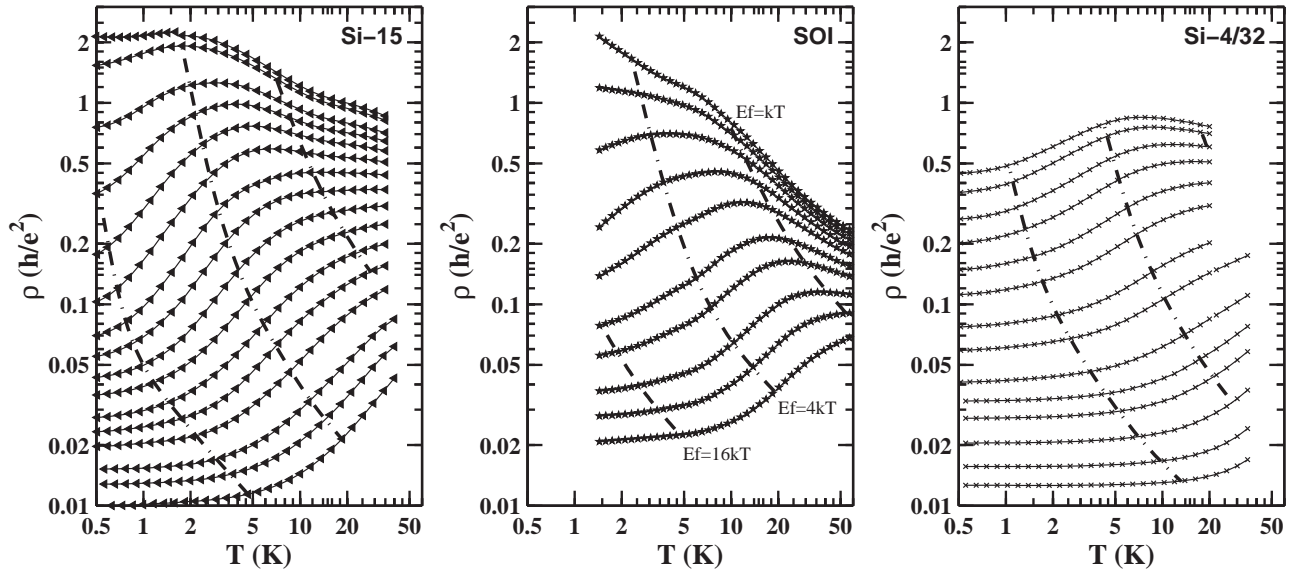


FIG. 3. Resistivity versus temperature behavior in units of  $h/e^2$  for a) high-mobility Si-MOS sample Si-15 ( $\mu_p = 2.7 \text{ m}^2/\text{Vs}$ ), b) SOI-L2 sample ( $1.17 \text{ m}^2/\text{Vs}$ ), and c) medium mobility Si-MOS Si-4/32 ( $0.8 \text{ m}^2/\text{Vs}$ ). The electron densities for Si-15 are between  $0.93$  and  $10.2 \times 10^{11} \text{ cm}^{-2}$ , for SOI-L2 are  $1.28, 1.44, 1.67, 2.02, 2.47, 3.26, 4.06, 5.65, 7.50$  and  $10.4 \times 10^{11} \text{ cm}^{-2}$  and for Si-4/32 between  $2.34$  and  $28.9 \times 10^{11} \text{ cm}^{-2}$ .

Figure 4 shows a direct comparison of the strong changes in  $\rho(T)$  for the four samples Si-15, Si-43, SOI-L2 and Si-4/32 for the same low- $T$  resistivity  $\rho = 0.0274h/e^2$ . The same behavior, as described above, is visible: the higher the peak mobility, the stronger is the change in  $\rho(T)$  and the lower is the temperature where the increase starts.

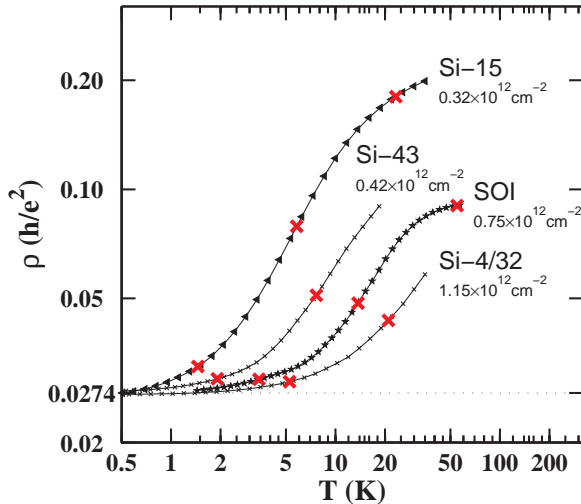


FIG. 4.  $\rho(T)$  for samples Si-15, Si-43, SOI-L2 and Si-4/32 for one and the same low- $T$  resistivity of  $0.0274h/e^2$ . The crosses on the curve from left to right mark the temperature where  $k_B T = E_F/16, E_F/4$ , and  $E_F$ .

For Si-MOS structures, it was shown that the critical conductance  $g_c = 1/\rho_c$  changes systematically with the

peak momentum relaxation time  $\tau_p = m^* \mu_p / e$ , which is a measure of the sample quality<sup>12</sup>. Here  $m^*$  denotes the effective conductivity mass which is the transverse mass of the two lower lying valleys of  $m_t^* = 0.19 m_e$  and  $e$  the elementary charge. For the SOI structure,  $g_c$  is about  $1.1e^2/h$  and is compared in Fig. 5 with the values for several Si-MOS samples<sup>12</sup>. It can be seen, that the  $g_c$ -value for SOI coincides quite well with the general behavior of the Si-MOS samples.

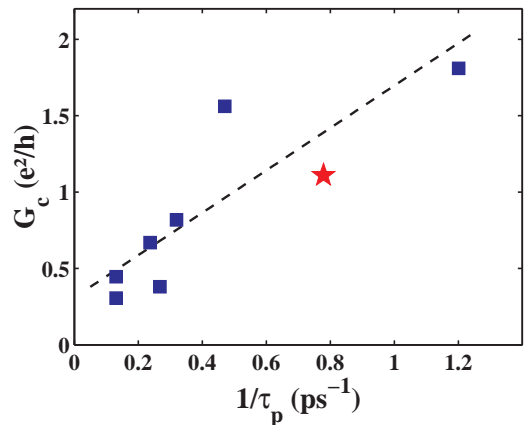


FIG. 5. Critical conductance  $g_c$  in units of  $e^2/h$  versus the inverse peak momentum relaxation time  $1/\tau_p$  for the SOI structure L2 (star symbol) and several Si-MOS samples (square symbols). The dashed line shows a linear regression curve.

As was seen so far, the SOI structure behaves very similar to a high mobility Si-MOS sample. Therefore, we ask the question: What are the similarities and differences between the two sample types? Due to the different effective masses  $m^*$  perpendicular to the Si/SiO<sub>2</sub> interfaces and due to strain effects, the six-fold conduction band (CB) degeneracy at the  $\Delta$ -points of bulk Si is lifted and only the two lower lying valleys with their longitudinal axis perpendicular to the 2D layer are occupied. The Si layer in SOI is only 60 nm thick, below there is the buried oxide layer, which constitutes also of a thermally grown oxide fabricated before the wafer bonding process. The active Si-layer has an n-type background doping of about  $10^{15} \text{ cm}^{-3}$  which freezes out at low  $T$ . In the Si-MOS samples, the electrons are confined in the surface inversion layer of a nominally p-type doped bulk Si crystal. Our high mobility Si-MOS samples were doped with an acceptor density of about  $2 \times 10^{15} \text{ cm}^{-3}$ .

Due to the applied gate voltage  $V_g$ , an approximately triangular potential well results for the electrons at the upper Si/SiO<sub>2</sub> interface. Nevertheless, the extension of the electronic wave function is different for the SOI and the Si-MOS structure due to the different background doping. In the n-type SOI structure, the Fermi level  $E_F$  is pinned underneath the 2D layer between the donor level and the CB edge. The band bending below the 2D layer is therefore quite small. In p-type Si-MOS, there is a wide depletion layer of about  $0.85 \mu\text{m}$  below the 2D layer, as  $E_F$  is pinned here between the acceptor level and the valence band (VB) edge in the undistorted p-type region. The different band bending below the 2D layer has an influence on the extension of the wave functions especially for small electron densities.

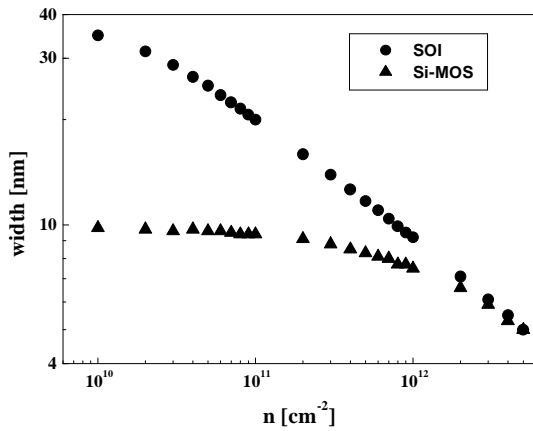


FIG. 6. Width of electron wavefunction versus electron density  $n$  for SOI (circle symbol) and Si-MOS (triangle). The width is defined to include the center 90 percent expectation probability of the wave function, 5 percent at the left and the right hand side are omitted.

We have calculated the wave function  $\Psi(z)$  and the triangular potential  $V(z)$  by solving the Schrödinger and

Poisson equations in a self consistent way (with  $z$  the coordinate perpendicular to the interface layer). In order to solve the Schrödinger equation, the charge distribution  $\rho(z) \propto |\Psi^2(z)|$  was taken into account. No exchange or correlation effects among the electrons were considered, thus giving a first order approximation of  $\Psi(z)$  and  $V(z)$ . Figure 6 shows the width of the wave function versus electron density  $n$ . The width of  $\Psi$  is defined as the length where the central 90 percent of the expectation probability  $|\Psi^2|$  is contained, with 5 percent at the left and at the right side ignored. For a high electron density of  $10^{12} \text{ cm}^{-2}$  the width is with 7.6 and 9.2 nm nearly the same for both structures.

At lower densities, the difference in the width of  $\Psi$  increases. The depletion width of  $0.85 \mu\text{m}$  at an acceptor density of  $2 \times 10^{15} \text{ cm}^{-3}$  corresponds to a 2D charge density of  $1.7 \times 10^{11} \text{ cm}^{-2}$ . Thus, at that 2D electron density, the electric field at the Si/SiO<sub>2</sub> interface is in Si-MOS twice as high as in the SOI structure. As can be seen from Fig. 6, the difference in the wave function extension is indeed large at that density. At still lower density, the width saturates in Si-MOS, as the field from the conducting 2D electrons is less important than that from the acceptors in the depletion layer. On the opposite, the width in the SOI structure further increases, as there is no electric field confinement from other charges than the conducting electrons itself.

Figure 7 shows for comparison the potential shape  $V(z)$  and the wave function  $\Psi(z)$  at  $n = 10^{11} \text{ cm}^{-2}$ . At that density, the confining potential is much steeper in Si-MOS and thus the energy  $E_0$  of the lowest electronic subband is with 31 meV much higher than in SOI with 14 meV. In Fig. 7, the difference in the width of the wave functions is also clearly visible and is caused by the difference in the potential steepness. For the case that higher subbands  $\Psi_n(z)$  are occupied, the differences in their energies and extensions should be even larger.

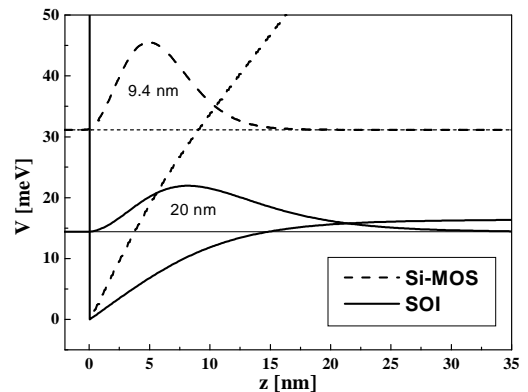


FIG. 7. Comparison of the wave functions  $\Psi(z)$  and the potential shape  $V(z)$  for the SOI (solid line) and Si-MOS structure (dashed line) at an electron density of  $1 \times 10^{11} \text{ cm}^{-2}$ .

In the considered density range, the width of the wave function is always smaller than the Si-layer thickness of the SOI structure and thus the electron do not feel the lower Si/SiO<sub>2</sub> interface towards the buried oxide layer. In order that such an effect could become significant, the Si layer would have to be as thin as 20 nm for  $n \approx 1 \times 10^{11} \text{ cm}^{-2}$  and even thinner for higher densities.

### C. Magnetoresistivity

We have also investigated the SOI structures in perpendicular and parallel (i.e. in-plane) magnetic field  $B$ . Figure 8 shows typical magnetoresistivity curves  $\rho_{xx}(B_{\perp})$  for  $B$  perpendicular to the 2D layer for different densities at  $T = 1.4 \text{ K}$ . For the lower densities, the weak localization peak around  $B = 0$  is clearly visible. At about 1 T, the Shubnikov - de Haas oscillations set in and gain strongly in amplitude towards higher magnetic fields. At around 4 T, the spin splitting is visible. The behavior in perpendicular magnetic field is again very similar to that of Si-MOS samples with comparable mobility.

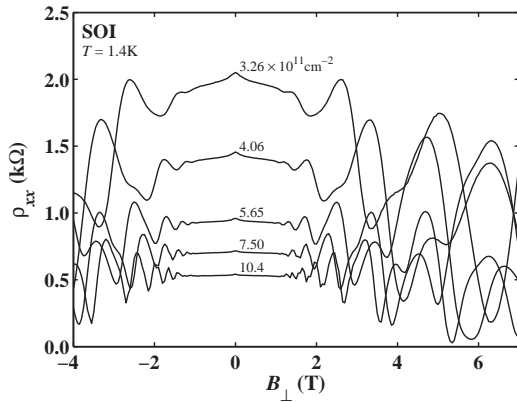


FIG. 8. Magnetoresistivity  $\rho_{xx}$  for magnetic fields oriented perpendicular to the 2D layer for  $n = 3.26, 4.06, 5.65, 7.50,$  and  $10.4 \times 10^{11} \text{ cm}^{-2}$  at a temperature of 1.4 K.

For in-plane magnetic field, the relative change  $\rho_{xx}(B_{\parallel})/\rho_{xx}(0)$  of the magnetoresistivity of SOI sample L2 is shown in Fig. 9 for different densities at  $T = 1.4 \text{ K}$ . At high densities of about  $1 \times 10^{12} \text{ cm}^{-2}$ , the changes are quite small, whereas for the lower densities there is a strong increase in  $\rho_{xx}$  by up to a factor 4. At the lowest density of  $1.28 \times 10^{11} \text{ cm}^{-2}$ , the observed change is again lower than for the previous densities as can be seen from the crossing of the upper curves in Fig. 9. This indicates a saturation of the strong increase in  $\rho_{xx}(B_{\parallel})$  at about  $1.5 \times 10^{11} \text{ cm}^{-2}$ .

An even stronger  $\rho(B_{\parallel})$ -dependence was observed in high-mobility Si-MOS structures in the metallic regime<sup>13,14</sup>. Again the changes were stronger for the lower densities  $n$ . The increase with  $B_{\parallel}$  was first attributed to the spin polarization of the conducting

electrons<sup>15</sup> and later to the increase in disorder caused by the magnetic field<sup>9</sup>. A strong change of  $\rho(B_{\parallel})$  was also observed in p-type GaAs/AlGaAs structures.<sup>16</sup>

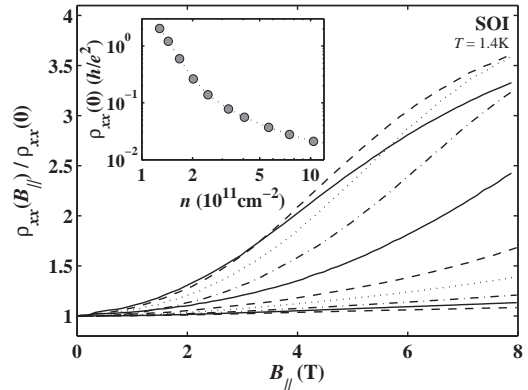


FIG. 9. Relative change of the magnetoresistivity  $\rho_{xx}(B_{\parallel})/\rho_{xx}(0)$  for magnetic fields oriented parallel to the 2D layer for  $n = 1.28, 1.44, 1.67, 2.02, 2.47, 3.26, 4.06, 5.65, 7.50,$  and  $10.4 \times 10^{11} \text{ cm}^{-2}$  (from top to bottom) at a temperature of 1.4 K.

## III. DISCUSSION

Above, we have presented new results on the 2D metallic state in silicon-on-insulator structures and compared its properties with that of high-mobility Si-MOS samples. As the physical origin of the 2D metallic state is still an open question, we like to discuss the different possibilities in detail.

There appear to remain five important suggestions for the 2D metallic state at low temperatures. These are (i) a new quantum mechanical ground state for electrons in a solid, (ii) scattering of electrons at charged hole traps in the oxide layer, (iii) interband scattering between different bands, (iv) temperature dependent screening of impurity scattering, and (v) coherent interaction corrections in the ballistic regime. If the first suggestion proves to be correct, the 2D MIT would indeed be the manifestation of some new physics, whereas the next three suggestions are based on settled physical phenomena, which may be described by terms like conventional, semiclassical or non-coherent (on the first sight). The fifth suggestion was proposed quite recently and it has to be discussed whether it can be classified in the terminology used above or not.

### A. New quantum mechanical ground state

The first suggestion (i) of a new quantum mechanical ground state is based on the scalability of the resistance in the neighborhood of the apparent MIT in

high-mobility Si-MOS structures<sup>1</sup>. It was found that the  $\rho(T, n)$ -curves for  $n < n_c$  and for  $n > n_c$  can be brought to coincidence on two distinct curves for the insulating and the metallic regime, respectively, by scaling the temperature with  $T/T_0(n)$ . The scaling parameter exhibits a power law  $T_0 \propto |\delta_n|^b$ , with  $\delta_n = (n - n_c)/n_c$  and  $b \approx 1.6$ . Such a critical scaling behavior indicates the metal-insulator transition to be a quantum phase transition<sup>20,19</sup>.

The seminal paper on the absence of quantum diffusion in two dimensions<sup>2</sup> was based on the assumption of non-interacting electrons. In this case the weak localization contribution decreases the conductivity and leads to continuing higher resistivities with decreasing temperatures. In the recent quantum-phase-transition models for the unexpected MIT in 2D, the electron-electron (e-e) interaction plays a dominant role<sup>17-20</sup>. The quantum coherent interaction corrections consist of positive and negative contributions to the conductivity and may lead to a decrease of the resistivity under certain conditions<sup>21</sup>. In any case, quantum coherence is a prerequisite that the MIT can be a quantum phase transition.

A metallic behavior, i.e. a strong drop in the resistivity, was not only observed in the near vicinity of the critical concentration  $n_c$  but also far away, for densities up to  $n > 1 \times 10^{12} \text{ cm}^{-2}$  (i.e. more than 10 times  $n_c$ ). As the decrease in  $\rho(T)$  looks quite similar near  $n_c$  and far away, it is quite instructive to look for quantum effects over an extended density range. In a recent work<sup>11</sup>, the temperature dependence of the weak localization was investigated in the metallic state of high-mobility Si-MOS structures in order to find the borders of quantum coherence. In that work, the temperature threshold  $T_q$  for the single-electron quantum coherence was deduced from the crossing point of the temperature dependence of the phase coherence time  $\tau_\varphi$  and the momentum relaxation time  $\tau$ . When  $\tau_\varphi > \tau$ , the coherence time is long enough that an electron can return in the coherent state to its origin whereas for  $\tau_\varphi < \tau$  this is not possible.

It was found for the Si-MOS system<sup>11</sup> that for  $n > 2 \times 10^{11} \text{ cm}^{-2}$ , the strong decrease in  $\rho(T)$  takes place above  $T_q$  and thus should not be related to a single-electron coherent effect. Also the second border  $k_B T_{ee} = \hbar/\tau$  lies below the strong resistivity drop at still higher densities. Therefore also the e-e interaction induced quantum corrections to conductivity should not be responsible for the resistivity drop in this regime. This should at least be deduced in the picture where quantum coherent effects and screening are attributed to two different physical phenomena. But recently an interesting paper by Zala et al. has appeared<sup>5</sup>, which may indicate that the two before mentioned effects are caused by the same physics. This will be discussed in more detail later in this work.

In any case, the work on the borders for quantum coherence<sup>11</sup> is strictly applicable only in the higher density regime and does not give a direct answer on the importance of quantum coherence in the close vicinity of the critical density  $n_c$ . In a recent work, Punnoose and

Finkelstein show<sup>21</sup> by a renormalization group analysis that especially for high-mobility Si-MOS structures, the presence of two degenerate conduction band valleys, stabilizes and enhances coherent e-e interaction effects in the vicinity of  $n_c$ . They are able to describe the temperature dependent changes in conductance in an  $n$ -range between  $0.83$  and  $0.94 \times 10^{11} \text{ cm}^{-2}$  without any adjustable parameter. So it is quite surprising that at low  $n$  the whole drop in  $\rho$  seems to come from quantum coherent interaction effects while at high  $n$  the drop takes place without quantum coherence and nevertheless the strong  $T$ -dependence looks so similar in the different regions. It is not yet clear whether the metallic and insulating behavior belong to a quantum phase transition or not. This work focuses on the metallic regime and will not be able to judge on the metal-to-insulator transition itself.

## B. Charged hole traps

The second suggestion (ii) on the scattering of electrons at charged hole traps in the oxide layer by Altshuler and Maslov (AM)<sup>30</sup> is prepared especially for Si-MOS structures with the Si/SiO<sub>2</sub> interface on the gated side of the 2D layer. The same model should be applicable also for our SOI structures, as an equivalent Si/SiO<sub>2</sub> interface is present for the 2D electron confinement.

It is well known that in the SiO<sub>2</sub> interface layer there exist several types of defects states<sup>32</sup>. In the AM model, it is assumed that a relative large number of hole trap states exists at a certain trap energy  $E_t$ , which is spatially homogeneously distributed in the oxide layer. It is further assumed that these trap states lie at a well defined energy  $E_{t0}$  if no external electric field is applied. The potential gradient due to an applied gate voltage  $V_g$  causes a linear increase of the trap energy position. In order to describe the total energy of the trap states, also the mirror charge of the traps inside the 2D electron gas has to be included. This leads to a down bending or the energetic position towards the interface and causes a maximum in the total trap energy  $E_t(z)$ , with  $z$  the position inside the oxide layer (see Fig. 18 in Appendix A). When the Fermi energy lies below certain trap states at energies  $E_t(z)$  (for low  $n$ ) these states are positively charged and cause a large scattering probability for the 2D electrons. At high densities all trap states lie below  $E_F$  and only due to the Boltzmann occupation tail, an exponentially small number of traps contributes to the electron scattering. The charged trap states form dipoles together with their mirror charge in the 2D layer which has to be taken into account in the calculation of the scattering cross section.

In order to calculate the resistivity, one needs to know how the Fermi energy  $E_F$  varies with the temperature  $T$  (in the work of AM, the chemical potential at  $T = 0$  is called the Fermi energy  $E_F$  whereas the chemical potential at  $T > 0$  is denoted by  $\mu(T)$ ; in this work we use

$E_F(T)$  instead). AM suggest two scenarios for the  $T$  dependence of the Fermi energy of the 2D electron gas : (a) it coincides with the Si substrate or (b) it is decoupled from the substrate.

For case (a), the calculation of  $\rho(T)$  by AM show a behavior which looks quite similar to the observed temperature dependence near the critical density  $n_c$  for high mobility Si-MOS structures. The strong increase in  $\rho$  with increasing  $T$  occurs around  $k_B T \approx E_F - E_t$  as then the occupied trap states are partially emptied (and charged) due to the broadening of the Fermi occupation function and the scattering rate is increased accordingly. For case (a), the insulating and metallic regions are distributed quite symmetrically around the separatrix which occurs for  $E_F = \max(E_t(z))$ .

For case (b), the resistivity is decreasing in both regimes ( $E_F \geq E_t$ ) according to the calculations of AM<sup>30</sup> and seems to be unable to explain the experimentally observed behavior. As mentioned by AM, the more realistic case is (b) as the depletion layer isolates the 2D electron gas from the substrate and both regions should have different quasi Fermi energies. This is also verified experimentally<sup>33</sup>. This situation causes some difficulty in order to apply the charge trap model to the high-mobility Si-MOS structures as well as to the SOI samples considered in this work.

We have performed numerical calculations of the AM-trap model for the SOI data. These calculations are described in appendix A in detail. If one applies an increasing gate voltage  $V_g$  in order to increase the electron density  $n$  in the 2D layer, the spatial maximum in the trap energy shifts quite fast to lower energies. This leads to a strong occupation of the trap states as soon as the maximum shifts below the Fermi energy  $E_F$  and the scattering efficiency decreases drastically. In Fig. 10, we have calculated the  $\rho(T)$  dependence at an intermediate temperature of  $T_i = 3.1$  K, where we have a set of measurement data. The temperature  $T_i$  was chosen so that  $\rho(n, T_i)$  is for a large density interval neither in the low- $T$  saturation nor in the “normal” high- $T$  regime. The resistivity behavior should be dominated by thermal excitation of carriers according to the AM-trap model. The low- $T$  saturation of  $\rho(T)$  in the metallic regime cannot be described with the AM-trap model alone, as all traps get filled according to the exponential Boltzmann-tail and the resistivity tends to zero. Only by assuming additional residual scattering centers, the resistivity saturates. We have evaluated the measurement data at  $T_i$  only for densities where the low- $T$  saturation should not have a large influence yet.

Figure 10 shows that the decrease in resistivity vs. density is too strong by many orders of magnitude in the AM-trap model. At  $n = 2.5 \times 10^{11} \text{ cm}^{-2}$ ,  $\rho$  should be below  $10^{-30} h/e^2$ . This low value results from a very small number of positively charged trap states according to the Fermi-Dirac occupation function. Temperature dependent screening effects were not considered in this calculation as they give only a change in  $\rho$  by one or two

orders of magnitude, but the calculated resistivity is by about 30 orders of magnitude too small compared with the measured values. In the same density interval, the measured resistivity decreases just by about one order of magnitude, which appears as a nearly flat line on the scale of Figure 10.

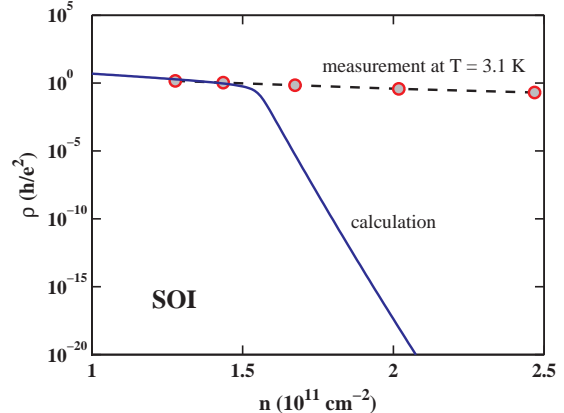


FIG. 10. Comparison of  $\rho(n)$  at  $T_i = 3.1$  K for experimental data (circles) and calculations (solid lines) according to the AM-trap model.

We conclude on the AM-trap model that it cannot explain the experimental behavior of the SOI (and similarly of the Si-MOS) samples at intermediate temperatures as the carrier freeze out on the trap states occurs by far too fast if the trap maximum is below  $E_F$ . Further improvements of the AM-model may be possible, but one has to note that the addition of trap states at other energies or the energetical broadening of the trap states around  $E_t$  destroys the critical behavior around  $n_c$  and the modified model would probably not be able to describe the abrupt metal to insulator transition.

Moreover, case (a) of the trap model by AM seems to be able to explain the  $\rho(T)$  dependence only in a very narrow density range around  $n_c$  but can not explain the metallic behavior for the wide  $n$  range as observed in Si-MOS and SOI samples. Thus it seems to be possible that the hole trap model in the present form may explain some important contributions to  $\rho(T)$  in Si-MOS and SOI but is unable to describe the whole temperature dependence. As mentioned above, the AM model is especially prepared for samples with an  $\text{SiO}_2$  oxide layer as on border of the 2D electron gas. The model will thus probably not be able to explain the metal-insulator transition in other material systems with strong changes in  $\rho(T)$  like p-type AlGaAs or Si/SiGe. On the other hand, it is not clear anyway whether the apparent metal-insulator phase transition has a universal origin or if it is caused by several different effects in the different material systems.

### C. Interband scattering

The third suggestion (iii) is attributed to interband scattering between different conduction or valence bands. The correlation between the existence of two conduction bands and the metallic behavior was proposed by Pudalov for Si-MOS.<sup>34</sup> He assumed that the spin-orbit coupling due to the asymmetry of the inversion layer potential is strong enough in order to create the splitting. But the calculation of the spin-orbit coupling is not straight forward and have to be performed with great care.<sup>35</sup> A later estimate by Pudalov et al.<sup>36</sup> gives a clearly smaller value for the spin-orbit coupling constant of  $\alpha \approx 6 \times 10^{-6}$  K cm, so that the corresponding splitting should not be the origin of the metallic behavior in Si-MOS structures. For p-type AlGaAs Papadakis et al. have argued<sup>37</sup> on the spin-orbit coupling due to the inversion asymmetry of the electron layer potential, but it turned out that the effect is due to an anomalous behavior of the magneto-oscillations<sup>38</sup>.

Nevertheless, the apparent metallic behavior in p-type AlGaAs layers strongly points towards a two-band transport effect.<sup>39</sup> There, the heavy hole band is split and inelastic interband Coulomb scattering between the two bands with different dispersion takes place. This was confirmed by magnetotransport measurements, where the positive magnetoresistance is attributed to the classical two-band scattering effect. But for n-type Si-based heterostructures, the two-band transport should not be of great importance, as the conduction band splitting seems to be rather small.

### D. Temperature dependent screening

The fourth suggestion (iv) on temperature dependent screening evolves from calculations of the mobility versus electron density dependence for Si-MOS<sup>22,23,10,7</sup>, Si/SiGe<sup>24</sup> and III-V<sup>25</sup> structures in the 80's. In these early works, the resulting  $\rho(T)$ -dependence was assumed to be relative small. The temperature dependence of the resistivity is dominated by the behavior of the screening function  $S(q)$ . For  $T = 0$ , this function has a distinct kink at  $q = 2k_F$  with  $k_F$  the Fermi wave vector. For higher  $T$ , this kink is smeared out<sup>22</sup> and changes the scattering efficiency especially for  $q = |\vec{k} - \vec{k}'| \approx 2k_F$ . Thus for large angle scattering, the temperature dependence of the screening function strongly influences the scattering efficiency.

Gold and Dolgoplov give analytic results for the screening<sup>7</sup> that consist of linear-in- $T$  and  $T^{3/2}$  terms

$$\delta\sigma(T) \approx -C(\alpha, n) \frac{k_B T}{E_f} - D(\alpha, n) \left[ \frac{k_B T}{E_f} \right]^{3/2}, \quad (1)$$

with  $C(\alpha, n) = 2C(\alpha)C(n)$ ,  $D(\alpha, n) = 2.45C(\alpha) [C(n)]^2$  and  $C(\alpha)$  a constant depending whether the scattering

is dominated by impurities ( $\alpha = -1$ ) or by surface-roughness ( $\alpha = 0$ ). We have fitted the  $\rho(T)$  behavior with the Eq. 1, assuming  $\alpha = -1$  and  $C(\alpha) = 2 \ln 2$ . The prefactor  $C(n)$  was used as a fitting parameter. As the analytic results are only valid for  $k_B T < E_F/4$ , the fit was limited to that range. Figure 11 shows that the fit gives a very good agreement with the observed  $T$  dependence.

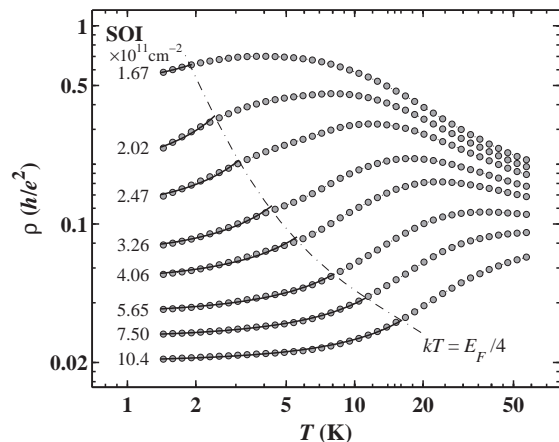


FIG. 11. Fit of the temperature dependent resistivity with  $T$  and  $T^{3/2}$  screening terms for  $k_B T < E_F/4$ .

The fitted prefactor  $C(n)$  increases from 0.4 at  $n = 10 \times 10^{11} \text{ cm}^{-2}$  to 0.55 at  $2 \times 10^{11} \text{ cm}^{-2}$ . For lower densities, the fit does not give reasonable results as the slope of  $\rho(T)$  changes sign at the critical density  $n_c$  which can not be described by the screening approximation alone. In Fig. 12, the range of the increase in  $C(n)$  towards lower densities is compared with the calculated behavior according to Gold and Dolgoplov<sup>7</sup>. As can be seen, there is good agreement with the curve of the local field correction parameter of  $G(2k_F) = 0.75$ . But if one inserts  $2k_F$  for  $q$  in  $G(q) = (1/2g_\nu)q/(q^2 + k_F^2)^{1/2}$  as given for Hubbard's approximation in Ref.<sup>7</sup>, one obtains  $G(2k_F) = 0.224$  (with  $g_\nu$  the valley degeneracy). Thus the above screening description is able to describe the temperature dependence but has to use a larger value for the local field correction parameter  $G(2k_F)$  as follows from the Hubbard approximation. This discrepancy possibly results from the fact that in local field correction parameter only exchange effects are taken into account and no correlation effects. But the latter might become important for large electron-electron interaction parameters  $r_s$ . The parameter  $r_s$  describes the ratio of Coulomb to kinetic energy and can be written as  $r_s = g_\nu/a_B\sqrt{\pi n}$ , with  $a_B$  the Bohr radius. Recently, Das Sarma and Hwang calculated<sup>26</sup> that due to temperature dependent screening, changes in  $\rho(T)$  by even up to one order in magnitude can be explained by numerical calculations.



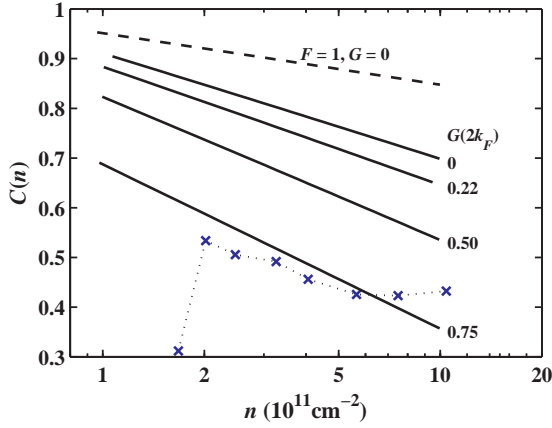


FIG. 12. Density dependence of the prefactor  $C(n)$  in the screening fit.

Another puzzling phenomenon in high-mobility Si-MOS structures, but also in the SOI samples investigated in this work and in other material systems, is the strong positive magnetoresistance in parallel magnetic field  $B_{\parallel}$ . In Si-MOS structures a more than ten-fold and in SOI a nearly four-fold increase in  $\rho(B_{\parallel})$  was observed. Dolgoplov and Gold calculated<sup>27</sup> that an increase of up to a factor 4 in  $\rho(B_{\parallel})$  can take place as the electron system becomes completely spin polarized. This strong increase is caused by changes in the density of states at  $E_F$ , in the Fermi wave vector  $k_F$  and in the screening wave number  $q_s$ <sup>27</sup>. We have fitted our data on SOI according to this theory, the results are shown in Fig. 13.

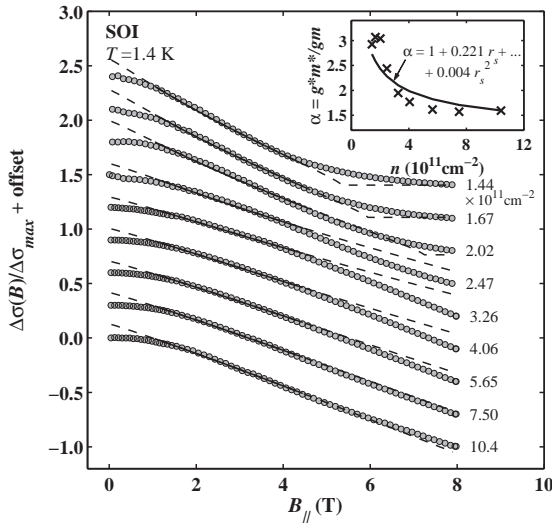


FIG. 13. Fit of the SOI magnetoresistivity  $\rho(B_{\parallel})$  with the screening behavior according to Dolgoplov and Gold. Densities are the same as in Fig. 9. The inset shows the density dependence of the ratio  $\alpha = g^*m^*/gm$  according to the performed fit (x-symbols) and to the literature (solid line).

As can be seen, at high electron densities (i.e. low resistivity) the fit in Fig. 13 is in good agreement with the data, whereas at lower densities (i.e. high resistivity and

strong changes in  $\rho(B_{\parallel})$ ), the screening behavior leads to curves which are rather linear and do not show the curvature of the measured values at low  $B_{\parallel}$  fields. For low density, at high  $B_{\parallel}$  fields, the model calculation shows an abrupt saturation of the resistivity which corresponds to the complete spin polarization of the electron system. Both discrepancies between calculation and measurement may be caused by the fact that the model<sup>27</sup> was formulated for  $T = 0$  K. In that case, the Fermi-Dirac distribution is a step function and leads to the kink at the  $B_{\parallel}$  saturation field. The approximately linear behavior of  $\rho(B_{\parallel})$  for small  $B_{\parallel}$  is probably caused by the distinct kink<sup>22</sup> in the screening function at zero  $T$ . For  $B = 0$  only one kink exists at  $q = 2k_F$  which splits into two kinks for  $B > 0$ .<sup>27</sup> At  $T > 0$ , the kinks in the screening function are rounded and thus a small splitting of the two screening functions (by  $B_{\parallel}$ ) for the spin up and spin down electron systems will not be so effective.

In order to fit the screening model to the data, an effective  $g^*$  factor was used as the only fitting parameter instead of a constant value for  $g$ . The resulting ratio  $\alpha = g^*m^*/gm$  is shown by cross symbols in the inset of Fig. 13 in comparison to the ratio  $\alpha$  from the analysis of Shubnikov-de Haas measurements on Si-MOS samples<sup>28</sup> (solid line). Over all, there is a good agreement between  $\alpha$  from the screening fit and the Si-MOS values. Just at the lowest  $n$ , the deviation is non-monotonic, but this may be caused by the large deviations in the calculated and measured  $\rho(B_{\parallel})$  values as the calculation is performed for  $T = 0$ . On the other hand, the above screening model<sup>27</sup> is also limited by the Hubbard approach, which does not take into account electronic correlation effects. A further work by Gold indicates<sup>29</sup> that even larger ratios of  $\rho(B_{\parallel} \geq B_c)/\rho(B = 0)$  than four can be explained beyond the random phase approximation by taking into account exchange/correlation (i.e. many body effects) and multiple scattering effects. In this framework possibly the data for high-mobility Si-MOS samples can be explained as well.

### E. Ballistic interaction corrections

The fifth and last suggestion (v) on the origin of the metallic state in 2D concerns coherent interaction corrections (CIC) to the conductivity in the ballistic regime. The theory for it was recently introduced by Zala, Narozhny, and Aleiner (ZNA)<sup>5</sup>. Previously, Altshuler and Aronov have calculated quantum corrections to conductivity (which include especially the interaction corrections) in the diffusive regime (i.e. at low temperatures, where  $k_B T \ll \hbar/\tau$ ) and found a typical  $\ln(T)$  behavior<sup>31</sup>. For the intermediate  $T$  range (i.e. the ballistic regime, where  $k_B T > \hbar/\tau$ ), ZNA found a linear in  $T$  contribution.<sup>5</sup> In addition, they calculated the coherent interaction corrections for the transition regime, where the behavior changes from diffusive to ballistic. In

the ballistic regime, the dominant processes can be understood as coherent backscattering of electrons at the Friedel oscillations of the other electrons around some perturbation centers.<sup>5</sup> In contrast, the coherent scattering in the diffusive regime occurs at two or more centers into a wider range of angles. In the approach of ZNA, where the interaction corrections are calculated in terms of the Fermi liquid parameter  $F_0^\sigma$ , correlation (Hartree) and exchange (Fock) terms are included. As the Fock terms have opposite sign to the Hartree terms and the relative strength of the two contributions varies with temperature and electron density, the resulting interaction corrections may be either positive or negative. The relation of the ballistic interaction correction to the former screening approach will be discussed later.

We have fitted the temperature dependence of the SOI-resistivity by the theory of ZNA, but adopting the situation for two-fold valley degeneracy in n-type Si inversion layers. As was shown by Punnoose and Finkelstein<sup>21</sup>, the valley degeneracy leads to 15 spin triplet channels instead of 3 for the one-valley situation. In both situations there is just one charge channel participating. This modification of the ZNA theory was also taken into account in the evaluation of the resistivity in Si-MOS by Vitkalov et al.<sup>41</sup> and Pudalov et al.<sup>42</sup>

In order to fit the experimental data  $\rho(T)$ , the functions  $f(T\tau)$  and  $t(T\tau; F_0^\sigma)$  for the charge and triplet channels, respectively, were calculated according to Ref.<sup>5</sup> and tabulated. The Fermi liquid parameter  $F_0^\sigma$  and the conductivity  $\sigma(T=0)$  are used as fitting parameters in a true multi-parameter least-square-fit procedure. As in the screening case (iv), the fit is performed for  $k_B T \leq E_F/4$ . It can be seen from Fig. 14 that the fitted curve (solid line) describes the experimental values (circle symbols) quite well. The inset of Fig. 14 shows the  $F_0^\sigma$ -values as obtained from the fitting procedure. In the density range of 2 to  $10.4 \times 10^{11} \text{ cm}^{-2}$  the  $F_0^\sigma$  values lie between  $-0.23$  and  $-0.31$ . For the lowest density of  $1.67 \times 10^{11} \text{ cm}^{-2}$ , we find a significantly higher value of  $F_0^\sigma = -0.18$ . As can be seen from Fig. 14, the fit was performed only in a short temperature interval and the fit is not so significant there. On the other hand, one sees also that slope of the  $T$ -dependence is indeed drastically changing and one eventually comes into a different regime of the sample behavior. For even lower electron densities the fit did not give any reasonable results as the sample finally becomes insulating below  $n \approx 1.5 \times 10^{11} \text{ cm}^{-2}$ .

In our fitting procedure, we use  $\sigma(0)$  as a fitting parameter. In the work ZNA<sup>5</sup> and of Vitkalov et al.<sup>41</sup>, it is suggested to perform a linear extrapolation of the resistivity  $\rho(T)$  towards zero  $T$ . But this has the disadvantage that the other contributions (e.g. logarithmic ones) may lead to an offset and the value obtained by the extrapolation towards zero is not the optimal one. As we have included the diffusive (i.e. logarithmic) terms in our fit, we find a discrepancy between the fitted value  $\sigma(0)$  and the one from the linear extrapolation. With our procedure, we get a better consistency for the fit.

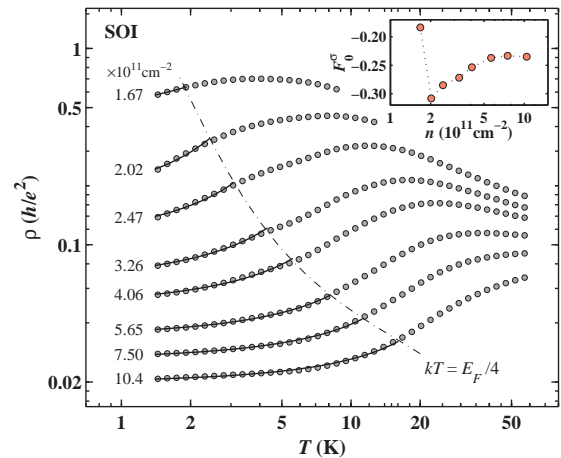


FIG. 14. Fit of the temperature dependent resistivity by the electron-electron interaction corrections in the ballistic regime according to Zala et al.

If we perform our fit on  $\rho(T)$  under the assumption of no valley degeneracy, then the resulting  $F_0^\sigma$  values have to be further negative and are typically in the range of  $-0.45$  to  $-0.5$ . This comes from the fact that the single charge channel is always localizing whereas the triplet channels contribute the delocalizing parts to the conductivity and the strength of the triplet channels increases towards negative values of  $F_0^\sigma$ . If there is just one valley present, the  $F_0^\sigma$  parameter has to be larger in order to lead to the experimentally observed delocalizing behavior towards low  $T$  whereas in the case of two valleys with 15 triplet channels, the  $F_0^\sigma$  value can be lower and still leads to the delocalizing behavior. For one valley the border between localizing/delocalizing behavior is given by  $F_0^\sigma \approx -0.4$ , for two valleys it is about  $-0.2$ . From the quality of the fit, it has to be mentioned that the screening fit of (ii) is nearly identical, the differences are very small. If one calculates the prefactor of the linear term in the ZNA theory and compares it with  $C(n)$  from the screening fit, one gets very similar values. This means that that in our case the Fock contribution seems to be not very important.

The interaction corrections at intermediate temperatures were also calculated for an in-plane magnetic field  $B_{\parallel}$  by ZNA.<sup>6</sup> Due to the bare Zeeman splitting  $E_z = g\mu_B B$ , the triplet states with different total spin component  $L_z$  are split and the interference effects (i.e. the triplet channels) are partly suppressed.<sup>6</sup> Note that one must not take the renormalized Zeeman splitting  $E_z^* = g^*\mu_B B$ , as homogeneous collective modes are not renormalized by electron-electron interaction.<sup>6</sup> We assumed again a two-fold valley degeneracy. In addition to the effective Zeeman splitting, a possible valley splitting also contributes to the conductivity corrections. The expression for the different corrections is given by<sup>41</sup>

$$\begin{aligned} \delta\sigma_{ee} = & \delta\sigma_C + 15\delta\sigma_T + 2\delta\sigma(E_z) + 2\delta\sigma(\Delta_V) \\ & + \delta\sigma(E_z + \Delta_V) + \delta\sigma(E_z - \Delta_V), \end{aligned} \quad (2)$$

where the terms correspond in the order of appearance to the charge and triplet channels, to Zeeman and valley splitting and to combinations of the latter two.

The behavior of the triplet states in parallel field and/or valley splitting is described by the functions  $K_b(x, F_0^\sigma)$  and  $K_d(x/\pi, F_0^\sigma)$  for the ballistic and diffusive case, respectively.<sup>6</sup> Here  $x = E_x/2T$  and  $E_x$  is any of the energies given as an argument in  $\delta\sigma$  of Eq. 2. We have again calculated and tabulated these functions in order to perform a true multi-parameter least-square fit procedure. First we describe a fit for  $\Delta_V = 0$ ; the case of  $\Delta_V > 0$  is discussed later. For the case of  $\Delta_V = 0$ , the conductivity corrections reduce to

$$\delta\sigma_{ee} = \delta\sigma_C + 15\delta\sigma_T + 4\delta\sigma(E_z). \quad (3)$$

Each  $\delta\sigma(E_z)$  is able to freeze two triplet channels  $2\delta\sigma_T$  (see Eq. 11 in ZNA<sup>6</sup>), so that in the high magnetic field limit  $E_z \gg k_B T$  only 7 triplet channels remain.

Figure 15 presents the result of the fit with  $F_0^\sigma$  and  $\rho(0)$  the fitting parameters and  $\Delta_V = 0$ . As can be seen from the figure there is a very good agreement for high densities over the entire  $B_{\parallel}$ -field rang and also for the lower densities for the low field part. At high parallel magnetic field and low density there is a discrepancy between calculations and experiment. This can be understood, as a limit of applicability of Eq. 2 is that  $E_z < E_F$ . For the lower electron densities in our experiment, we reach the total spin polarization regime and the latter relation is not fulfilled any more. At first we fitted the whole  $B_{\parallel}$ -range, but after recognizing the deviations at high fields, we limit the fit range to  $B_{\parallel} < 4$  T as is shown by the full lines in Fig. 15. The extrapolated  $\rho(B_{\parallel})$  behavior is indicated by the dashed part of the lines.

The inset of Fig. 15 depicts the obtained values for the fitting parameter  $F_0^\sigma$ , which are in the range of  $-0.21$  to  $-0.28$  for the higher electron densities. For the lower densities, we find a sudden upturn of  $F_0^\sigma(n)$ . It occurs for the same densities, for which there is a large and systematic deviation at high magnetic fields. Possibly, we reach a limit of the applicability of the theory.

We have also performed a least square fit with the additional fitting parameter  $\Delta_V$  for the valley splitting. We get values between  $\approx 0$  and 2 K for  $\Delta_V$ . These values do not depend systematically on  $n$ , but are rather scattered around in the before mentioned range – the significance of the parameter  $\Delta_V$  is very low. If we set  $\Delta_V = 0$ , as used for the fit above, the deviation of the fitted curve from the data points is nearly the same and the fitted values of  $F_0^\sigma$  and  $\rho(0)$  change only marginally. This means that we do not get a reasonable estimate for  $\Delta_V$  from the fit of our magnetoresistivity data for in-plane magnetic field.

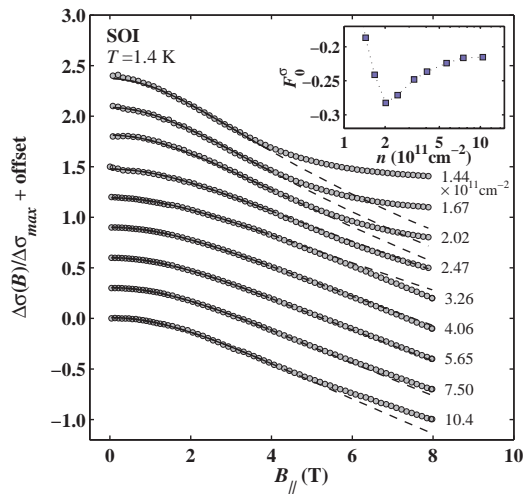


FIG. 15. Fit of the SOI magnetoresistivity  $\rho(B_{\parallel})$  with electron-electron interaction corrections in the ballistic regime according to Zala et al. Densities are the same as in Fig. 9. The inset shows the Fermi liquid parameter  $F_0^\sigma$  (circle symbols) in comparison to the values calculated from the effective g-factor in Si-MOS (solid line).

Figure 16 shows a comparison of the  $F_0^\sigma$  values as obtained from the fits of the  $T$ - and the  $B_{\parallel}$ -dependence. In the electron density range of 2 to  $6 \times 10^{11} \text{ cm}^{-2}$ , the values (marked by circles and squares) are close together. This means that two independent measurements and fits lead to very similar Fermi liquid parameters  $F_0^\sigma$ . This observation supports the validity of the ballistic interaction theory. For  $n < 2 \times 10^{11} \text{ cm}^{-2}$ , the  $F_0^\sigma$  values suddenly increase strongly. It seems that in this regime the description of the experiment by the interaction corrections in the ballistic regime breaks down. This is in good agreement with the observation in Si-MOS, that for  $n < 2 \times 10^{11} \text{ cm}^{-2}$ , the strong decrease in  $\rho(T)$  towards lower  $T$  is in the diffusive regime, so that the ballistic regime is active only for higher electron densities.<sup>11</sup> For comparison,  $F_0^\sigma$  was also calculated and plotted for high-mobility Si-MOS structures (solid line) as obtained<sup>28</sup> from the effective  $g^*$ -factor by the relation  $g^* = 2/(F_0^\sigma + 1)$ . The  $F_0^\sigma$  values obtained by the two different methods show the same trend in that they increase towards negative values for decreasing electron density, although the value appears to be more negative for Si-MOS. This discrepancy is not clear at the moment.

If one compares the fit of our SOI magnetoresistance data by the theory on interaction corrections at intermediate temperatures (ZNA)<sup>6</sup> with the theory on temperature dependent screening (Dolgoplov and Gold)<sup>27</sup>, it can be seen that the former theory gives a better description of the experimental data at low magnetic fields. In the first case, the nearly parabolic dependence of  $\rho(B_{\parallel})$  around  $B = 0$  is described well, whereas in the second case the fit gives a nearly linear  $B_{\parallel}$ -dependence. But as discussed earlier in this work, this is not astonishing, as the theory on screening in parallel fields is worked out so

far for  $T = 0$ , where the screening function has the well defined kink at  $q = 2k_F$ .

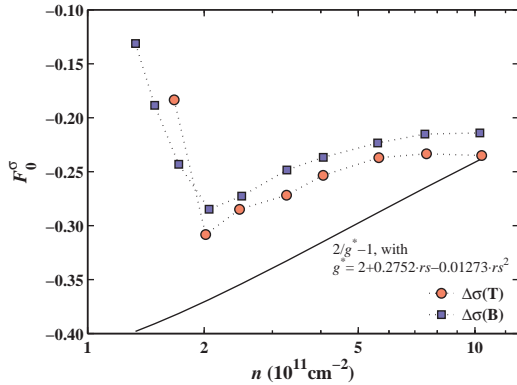


FIG. 16. Comparison of the Fermi liquid parameter  $F_0^\sigma$  as obtained from the fit of the temperature dependence (circles) and the in-plane magnetic field dependence (squares) of the SOI resistivity.

#### F. On a possibly new ground state

The first suggestion (i) on a new quantum mechanical ground state in the metallic regime should be discussed once more in the light of screening and coherent electron transport in the ballistic regime. In a recent work<sup>11</sup>, we concluded that the metallic state in Si-MOS samples is not caused by quantum coherent effects. We discussed screening as a prominent candidate for the metallic effect. At this time screening was not considered as a quantum coherent effect, primarily. In the new sight of ZNA, screening can be described by coherent back scattering of electrons at the perturbation centers and it's Friedel oscillations. It seems like suddenly the effect has changed it's habits.

If we now try to describe the strong resistivity decrease in a combined picture of screening and coherent ballistic contributions (let's denote it coherent screening regime), one should say that the correlation (Fock) contribution may give an important contribution and was missed in the former screening descriptions<sup>22,23,7</sup>. Only in some later work, the correlation contributions were included in the local field contribution<sup>29,43</sup>. On the other hand, the effect still reflects the behavior of the screening function with it's sharp kink at  $T = 0$  which is rounded for  $T > 0$ . In any case, the coherent screening effects leads to a linear  $T$  behavior and no new or extraordinary effects will emerge from itself.

The important realization is that the coherent conductivity corrections in the diffusive regime can be understood as a natural continuation of the coherent screening. It becomes important as soon as the coherent scattering extends over more than one scattering center at a time (which is known since many years). The diffusive regime describes the weak localization effect

and the coherent disorder-induced electron-electron interaction corrections.<sup>31</sup> Only if the latter contributions lead to strong and dominant conductivity corrections, one should speak of a new quantum mechanical ground state. Such a scenario was described by Punnoose and Finkelstein<sup>21</sup> in the case of two degenerate valleys where the delocalizing effect of the 15 triplet channels can be significantly enhanced due to renormalization effects. But this is not the case for higher electron densities of  $n > 2 \times 10^{11} \text{ cm}^{-2}$  as was shown in the recent work on the borders for quantum effects in the diffusive regime.<sup>11</sup> Only for lower electron densities, such a renormalization effect could significantly increase the delocalizing contributions and lead to a new ground state.

#### IV. SUMMARY

In conclusion, we have shown that silicon-on-insulator structures show a very similar 2D-metallic state as Si-MOS structures with comparable peak mobility. We discussed and compared several models on the physical origin of the metallic state. The theory on coherent interaction corrections at intermediate temperatures is able to describe the observed temperature and in-plane magnetic field behavior over a wide density range. Under the assumption of a two-fold valley degeneracy, the Fermi-liquid parameter  $F_0^\sigma$  is between  $-0.21$  and  $-0.31$ . The derivated Fermi-liquid parameters from the temperature and the in-plane magnetic field dependence are in very good agreement to each other. This observation points to the validity of the ballistic interaction theory. We do not get a significant influence from the valley splitting parameter  $\Delta_V$ . The earlier screening approach gives also a similarly good description for intermediate temperatures. This indicates that the correlation (or Fock) terms may not be very significant in the investigated regime. The charged trap state model, as given in the literature, is not able to describe the resistivity versus density behavior further away from the critical density of the metal-to-insulator transition. Also the two-band transport model seems to be not applicable for electrons in Si-layers. It is not clear yet whether there exists a true metallic state for low temperatures at low electron densities or not.

#### ACKNOWLEDGMENTS

We thank B.L. Altshuler, I. Aleiner, V.T. Dolgoplov, K. Ensslin, A. Finkelstein, A. Gold, B. Narozhny, D.L. Maslov, and V.M. Pudalov for stimulating discussions. The work was supported by the Austrian Science Fund (FWF) on the "Metallic State in 2D Systems".

## APPENDIX A: TRAP-MODEL CALCULATIONS

Analytic results for the metal-insulator transition in gated semiconductors according to trap states were calculated recently by Altshuler and Maslov (AM)<sup>30</sup>. In this work, AM assume that a hole trap exists in the oxide layer, which can easily be charged and discharged. The trap state is homogeneously distributed in space but has a distinct energetical position. Some of the equations used by AM were not derived in that work according to the length limits of the letter publication and in addition several approximations were used there. We find it therefore useful to discuss the calculations and our numerical results in more detail here.

Figure 17 shows a simple scheme of the hole trap states. If the chemical potential  $\mu$  (we use here now the same notation as by AM<sup>30</sup>) is below the trap state energy  $\varepsilon_t$  (Fig. 17a), a hole is trapped, it is positively charged and acts as an efficient scattering center. For the case that  $\mu$  is above  $\varepsilon_t$ , the center is neutral and is inefficient for scattering.

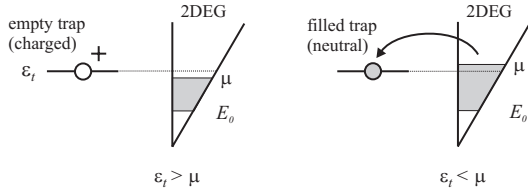


FIG. 17. Schematic representation of a hole trap center in relation to the 2D electron gas. For  $\mu < \varepsilon_t$  the trap state is positively charged whereas for  $\mu > \varepsilon_t$  the trap are neutral and do not act as scattering centers.

For the scattering centers, a dipole approximation is used by AM. It is assumed that a charge in the oxide layer will introduce an opposite mirror charge in the 2D layer due to screening on in-plane electric fields. For the energetical position of the trap state, a term  $e^2/(8\pi\epsilon_0\epsilon_{\text{ox}}z)$  has to be taken into account, with  $\epsilon_0 = 8.854 \times 10^{12} \text{ C}^2/\text{Nm}^2$  the vacuum permeability,  $\epsilon_{\text{ox}}$  the relative dielectric constant of the oxide and  $z$  the distance of the charge from the 2D electron layer; the calculations are performed in SI units here. The energetical position of the charged trap states also depends on the applied gate voltage via  $eV_g z/d$ , with  $d$  the thickness of the oxide layer. Figure 18 depicts the dependence of the total energy of the charged trap states in the dipole approximation as a function of the distance  $z$  for different gate voltages  $V_g$ . Only in the spacial region where  $\varepsilon_t(z) > \mu$ , the centers are positively charged.

The expression for the resistivity  $\rho$  follows in the Drude-Boltzmann approximation by calculating the effective transport scattering time

$$\langle \tau \rangle = \frac{\int d\varepsilon \tau(\varepsilon) \varepsilon \partial f / \partial \varepsilon}{\int d\varepsilon \varepsilon \partial f / \partial \varepsilon} \quad (\text{A1})$$

for the conductivity  $\sigma = ne^2 \langle \tau \rangle / m^*$ . The weighting of  $\langle \tau \rangle$  with the kinetic electron energy  $\varepsilon$  in Eq. A1 fundamentally follows from the Drude-Boltzmann approximation<sup>40</sup>, as the Fermi velocity  $v_F$  and the shift of the Fermi surface in k-space are both proportional to  $\sqrt{\varepsilon}$ , which enter into the expression for the current  $j_x = -e \int d\vec{k} n(\vec{k}) f(\varepsilon) v_x$ . The integral in the denominator of Eq. A1 is in 2D just equal to the Fermi energy  $E_F$  – also for elevated temperatures.

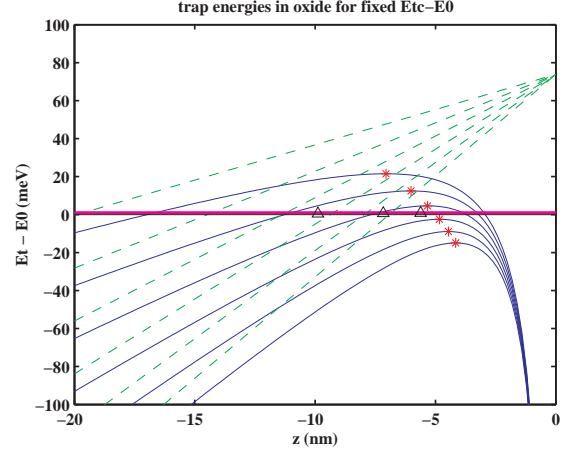


FIG. 18. Full lines show trap energy vs. distance  $z$  from the 2D electron gas layer plotted for different gate voltages  $V_g$ . The dashed lines indicate the potential energy of the trap without the mirror charge term; they merge on the right hand side at the trap energy  $\varepsilon_{t0}$ . The thick horizontal line indicates the position of the Fermi energy  $E_F$ ; it actually consists of several thin lines for different values of  $E_F(V_g)$ , but as the Fermi energies are so small in comparison to the considered trap energies, they are not resolved. The stars depict the maxima of the energy trap curves, the triangles show the mean  $z$ -value of the positive region, i.e. where  $\varepsilon_t > \varepsilon_0$  with  $\varepsilon_0$  the lowest 2D energy level in the Si inversion layer.

The transport scattering time  $\tau(\varepsilon)$  has to be calculated from the scattering rate

$$1/\tau(\varepsilon) = \int_0^d dz N_{t3}^+(z) v(\varepsilon) \sigma_{\text{scm}}(\varepsilon, z) \quad (\text{A2})$$

with  $N_{t3}^+(z)$  the three dimensional density of charged traps,  $v(\varepsilon)$  the electron velocity and  $\sigma_{\text{scm}}(\varepsilon, z)$  the scattering cross section for momentum relaxation. According to AM, the scattering cross section for a dipole is given by  $\sigma_{\text{scm}}(\varepsilon, z) = 2.74(e^2 z^2 / 8\pi\epsilon_0 \epsilon^* \varepsilon)^{1/3}$ . The effective relative permittivity  $\epsilon^* = (\epsilon_{\text{Si}} + \epsilon_{\text{ox}})/2 \approx 7.9$  is the mean value of the Si and the SiO<sub>2</sub> layer. The density  $N_{t3}^+(z) = N_{t3} P_+(z)$  in the AM notation with  $N_{t3}$  a constant density of traps per volume and  $P_+(z) = [0.5 \exp((\mu - \varepsilon_c(z) - \varepsilon_t)/k_B T) + 1]^{-1}$ , the thermodynamic probability for a trap state to be charged<sup>30</sup>.

By inserting the above expressions into Eq. A2 one gets

$$1/\tau(\varepsilon) = c' N_{\text{eff}}^+ z_m^{2/3} \varepsilon^{1/6} \quad (\text{A3})$$

with the factor  $c' = 2.74(e^2/8\pi\epsilon_0\epsilon^*)^{1/3}\sqrt{2/m^*}$ , an effective number of positive trap states per area  $N_{\text{eff}}^+ = N_{t3} \langle \Delta z \rangle_{\text{eff}}$ , the effective width of positive charge layer  $\langle \Delta z \rangle_{\text{eff}} = \int dz P_+(z)(z/z_m)^{2/3}$  and the position  $z_m = \sqrt{ed/8\pi\epsilon_0\epsilon_{ox}V_g}$  of the energetical maximum of the trap energy<sup>30</sup>. By inserting Eq. A3 into Eq. A1, one gets

$$\langle \tau \rangle \propto 1/\mu \int_0^\infty d\varepsilon \varepsilon^{5/6} \partial f / \partial \varepsilon. \quad (\text{A4})$$

For the Drude resistivity  $\rho = m^*/ne^2 \langle \tau \rangle$ , an effective energy  $\bar{\varepsilon}$  can be defined so that a relation equivalent to Eq. A3 can be written for the effective values, i.e.  $1/\langle \tau \rangle = c' N_{\text{eff}}^+ z_m^{2/3} \bar{\varepsilon}^{1/6}$ . A simple calculation gives

$$\bar{\varepsilon} = \mu^6 \left[ \int_0^\infty d\varepsilon \varepsilon^{5/6} \partial f / \partial \varepsilon \right]^{-6}. \quad (\text{A5})$$

The first derivative of the Fermi-Dirac function  $f$  can be expressed as

$$\begin{aligned} \partial f / \partial \varepsilon &= -f(1-f) \\ &= -(4k_B T \cosh^2((\varepsilon - \mu)/2k_B T))^{-1} \end{aligned} \quad (\text{A6})$$

and one obtains the same expression as Eq. 8 in Ref.<sup>30</sup> With these relations, the resistivity can exactly be written in terms of the effective energy  $\bar{\varepsilon}$  as

$$\rho = \frac{m^*}{ne^2} N^+ v(\bar{\varepsilon}) \sigma_{\text{scm}}(\bar{\varepsilon}, z_m). \quad (\text{A7})$$

We have calculate the resistivity  $\rho(n, T)$  by numerical integration for the effective thickness  $\Delta z$  of the layer with charged trap states and the effective energy  $\bar{\varepsilon}$ . In the work of AM<sup>30</sup>, a parabolic approximation was used for the dependence of the trap energy  $\varepsilon_t$  on  $z$  and an analytic expansion was given for the behavior of  $\rho(n, T)$ . With this, AM were able to show that in principle a critical behavior in the density dependence of  $\rho(T)$  can appear. As in our work, we want to test whether the metallic behavior can be explained for a wide density range or not, we use the numerical calculation method in order to be able to perform a precise evaluation of the model behavior for large deviations of  $n$  from the critical density  $n_c$ .

AM proposed in their model that the dependence of  $\rho(n)$  in the vicinity of  $n_c$  comes from the strong change of the number of positively charged centers, as the Fermi energy is just above or below the energy maximum  $\varepsilon_m$  of the trap states, where they have a singularity in the density of states. The sensitivity on temperature comes from the broadening of the thermodynamic probability distribution  $P_+$  with increasing temperature. In order to test this behavior for the strong temperature dependence of the resistivity, i.e. the most characteristic feature of the metallic state, we calculated the temperature dependence within the model at an intermediate temperature of  $T = 3$  K. For densities  $n < 5 \times 10^{11} \text{ cm}^{-2}$ ,  $\rho(T)$  does

not saturate yet at its low- $T$  value. The saturation behavior is not described by the AM-model. The low- $T$  value has to be caused by other mechanisms like residual impurities which do not change their charge state in the same manner. For the evaluated value of  $T \approx 3$  K, the  $T$ -dependence should behave according to the AM-model if it is able to describe the metallic state.

The result of our numerical calculation is shown in Fig. 10. It is clearly visible there, that the calculated  $\rho$ -dependence changes by many more orders of magnitude than the measured one. In order to analyze the origin of the strong change in the calculated  $\rho(n)$  behavior, we show in Fig. 19 the dependence of the effective number of charged trap states per area  $N_{\text{eff}}^+$  on the electron density (i.e. the gate voltage  $V_g$ ). As long as  $\varepsilon_m > \mu$  a part of the trap states is positively charged even for  $T = 0$  and the variation in effective positive charge layer width  $\Delta z$  is small. But for  $\varepsilon_m < \mu$ , the trap states are only charged according to the exponentially decaying part of the thermodynamic probability function  $P_+(z)$  and thus the strong exponential  $T$ -dependence occurs.

In the same density range, the other values which enter into the resistivity calculation (see Eq. A7) change only by about a factor of two. It is thus clear that within the proposed AM model, the strong shift of the energetical position of the trap states with the applied gate voltages leads to too strong changes in  $\rho(n)$  further away from the critical density  $n_c$ .

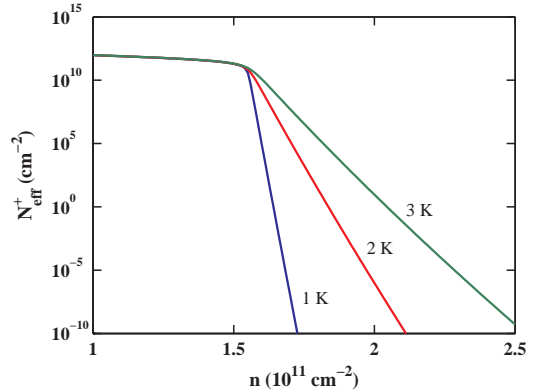


FIG. 19. Effective number of charged trap states per area  $N_{\text{eff}}^+$  vs. electrons density (i.e. varying gate voltage) at temperatures of  $T = 1, 3,$  and  $5$  K.

<sup>1</sup> S. V. Kravchenko, et al. Phys. Rev. B **50**, 8039 (1994); Phys. Rev. B **51**, 7038 (1995).

<sup>2</sup> E. Abrahams, P. W. Anderson, D. C. Licciardello, and T. V. Ramakrishnan, Phys. Rev. Lett. **42**, 673 (1979).

<sup>3</sup> D. Popovic, A. B. Fowler, and S. Washburn, Phys. Rev. Lett. **79**, 1543 (1997).

- <sup>4</sup> E. Abrahams, S. V. Kravchenko, and M. P. Sarachik, Rev. Mod. Phys. **73**, 251 (2001).
- <sup>5</sup> G. Zala, B. N. Narozhny, and I. L. Aleiner, Phys. Rev. B **64**, 214204 (2001).
- <sup>6</sup> G. Zala, B. N. Narozhny, and I. L. Aleiner, Phys. Rev. B **65**, 020201(R) (2001).
- <sup>7</sup> A. Gold and V. T. Dolgoplov, Phys. Rev. B **33**, 1076 (1986).
- <sup>8</sup> M. Bruel, MRS Bull. **23**, 35 (1998).
- <sup>9</sup> V. M. Pudalov, G. Brunthaler, A. Prinz, and G. Bauer, cond-mat/0103087.
- <sup>10</sup> A. Gold, Phys. Rev. Lett. **54**, 1079 (1985).
- <sup>11</sup> G. Brunthaler, A. Prinz, G. Bauer, and V. M. Pudalov, Phys. Rev. Lett. **87**, 096802 (2001).
- <sup>12</sup> V. M. Pudalov, G. Brunthaler, A. Prinz, and G. Bauer, Physica E **3**, 79 (1998).
- <sup>13</sup> V. M. Pudalov, G. Brunthaler, A. Prinz, and G. Bauer, JETP Lett. **65**, 932 (1997).
- <sup>14</sup> D. Simonian, S. V. Kravchenko, M. P. Sarachik, and V. M. Pudalov, Phys. Rev. Lett. **79**, 2304 (1997).
- <sup>15</sup> T. Okamoto, K. Hosoya S. Kawaji, and A. Yagi, Phys. Rev. Lett. **82**, 3875 (1999).
- <sup>16</sup> J. Yoon et al., Phys. Rev. Lett. **84**, 4421 (2000).
- <sup>17</sup> A. M. Finkelstein, Z. Phys. B: Condens. Matter **56**, 189 (1984).
- <sup>18</sup> C. Castellani, C. Di Castro, P. A. Lee, and M. Ma, Phys. Rev. B **30**, 527 (1984).
- <sup>19</sup> E. Abrahams and G. Kotliar, Science **274**, 1853 (1996).
- <sup>20</sup> V. Dobrosavljević, E. Abrahams, E. Mirinda, and S. Chakravarty, Phys. Rev. Lett. **79**, 455 (1997).
- <sup>21</sup> A. Punnoose and A. M. Finkelstein, Phys. Rev. Lett. **88**, 016802 (2002).
- <sup>22</sup> F. Stern, Phys. Rev. Lett. **44**, 1469 (1980).
- <sup>23</sup> S. Das Sarma, Phys. Rev. B **33**, 5401 (1986).
- <sup>24</sup> A. Gold, Phys. Rev. B **35**, 723 (1987).
- <sup>25</sup> A. Gold, Phys. Rev. B **38**, 10798 (1988), and Phys. Rev. B **41**, 8537 (1990).
- <sup>26</sup> S. Das Sarma and E. H. Hwang, Phys. Rev. Lett. **83**, 164 (1999).
- <sup>27</sup> V. T. Dolgoplov and A. Gold, JETP Lett. **71**, 27 (2000).
- <sup>28</sup> V. M. Pudalov et al., Phys. Rev. Lett. **88**, 196404 (2002).
- <sup>29</sup> A. Gold, JETP Lett. **72**, 401 (2000).
- <sup>30</sup> B. L. Altshuler and D. L. Maslov, Phys. Rev. Lett. **82**, 145 (1999).
- <sup>31</sup> B. L. Altshuler and A. G. Aronov, in *Electron-Electron Interaction in Disordered Systems*, edited by A. L. Efros and M. Pollak, North Holland, Amsterdam, 1985, p. 1.
- <sup>32</sup> “*Physics of Semiconductor Devices*”, S. M. Sze, John Wiley & Sons, New York 1981, p. 379.
- <sup>33</sup> T. Ando, A. B. Fowler, and F. Stern, Rev. Mod. Phys. **54**, 437 (1982), see p. 478.
- <sup>34</sup> V. M. Pudalov, JETP Lett. **66**, 175 (1997).
- <sup>35</sup> P. Pfeffer and W. Zawadzki, Phys. Rev. B **59**, R5312 (1999). W. Zawadzki and P. Pfeffer, Phys. Rev. B **64**, 235313 (2001).
- <sup>36</sup> V. M. Pudalov, G. Brunthaler, A. Prinz, and G. Bauer, Phys. Rev. Lett. **88**, 076401 (2002); see ref. 26 therein.
- <sup>37</sup> S. J. Papadakis et al., Science **283**, 2056 (1999).
- <sup>38</sup> R. Winkler, S. J. Papadakis, E. P. De Poortere, and M. Shayegan, Phys. Rev. Lett. **84**, 713 (2000).
- <sup>39</sup> Y. Yaish et al., Phys. Rev. Lett. **84**, 4954 (2000).
- <sup>40</sup> “*Semiconductors*”, R. A. Smith, Cambridge University Press, Cambridge 1964.
- <sup>41</sup> S. A. Vitkalov et al., cond-mat/0204566.
- <sup>42</sup> V. M. Pudalov et al., cond-mat/0205449.
- <sup>43</sup> A. Gold, J. Phys.: Condens. Matter **13**, 11641 (2001).